

Molecular Insights into the Translesion Synthesis of Benzyl-Guanine from Molecular Dynamics Simulations: Structural Evidence for Mutagenic and Nonmutagenic Replication

Katie A. Wilson and Stacey D. Wetmore*

Department of Chemistry and Biochemistry, University of Lethbridge, 4401 University Drive West, Lethbridge, Alberta T1K 3M4, Canada

*E-mail: stacey.wetmore@uleth.ca. Tel.: (403) 329-2323. Fax: (403) 329-2057.

Supplementary Information

Full Methods	S2
Figure S1. Modified hydrogen bonding for O6-dG alkylation adducts.....	S5
Figure S2. Geometry of dG:dCTP in the Dpo4 active site from a 100 ns MD simulation	S6
Figure S3. Geometry of Bz-dG:dCTP in the Dpo4 active site from a 100 ns MD simulation	S7
Figure S4. Proposed reaction mechanism	S8
Figure S5. Proposed hydrogen-bonding interactions.....	S9
Figure S6. Active site interactions between the dNTP and Arg51, and Lys159	S10
Figure S7. Active site interactions between the dNTP and Tyr12	S11
Figure S8. Overlay of hydrogen-bonding configurations	S12
Figure S9. Alternative <i>anti</i> -Bz-dG:dTTP hydrogen-bonding configuration	S13
Figure S10. Active site interactions between the dNTP and Tyr12, Arg51, and Lys159 in the ternary deletion complexes.....	S14
Table S1. Backbone rmsds throughout the simulations on the ternary complexes	S15
Table S2. Structural parameters in the ternary insertion complexes.....	S16
Table S3. Flanking base pair hydrogen bonding in the ternary complexes.....	S17
Table S4. Stacking and hydrogen-bonding energies for DNA–DNA interactions in the ternary insertion complexes	S18
Table S5. DNA– polymerase hydrogen-bonding interactions in the ternary insertion complexes	S19
Table S6. Free energies of DNA–DNA and DNA–polymerase interactions.....	S20
Table S7. Coordination of the catalytic Mg ²⁺ ions in the ternary complexes	S21
Table S8. Structural parameters in the ternary deletion complexes	S22
Table S9. Stacking and hydrogen-bonding energies for DNA–DNA interactions in the ternary deletion complexes	S23
Table S10. DNA–polymerase hydrogen-bonding interactions in the ternary deletion complexes	S24

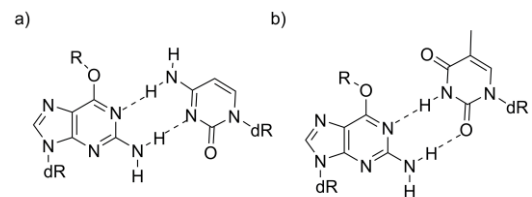
Full Methods

Starting Geometries: Initial structures for the MD simulations were obtained from chains B, E and F of a crystal structure of the Dpo4 ternary complex corresponding to the pairing of dATP opposite the 5'-dT with respect to the benzo[a]pyrene adenine adduct (PDB ID: 1S0M).⁴⁶ This crystal structure was chosen due to the presence of a dNTP (rather than a ddNTP), the near perfect coordination sphere of the catalytic divalent ions, and the lack of active site distortions. Two excess divalent ions (Ca405 and Ca408) were removed and the two remaining divalent ions (Ca403 and Ca404) were changed to the catalytic Mg²⁺ ions. We note that the position of the Mg²⁺ ions changes upon equilibration relative to the crystallographic Ca²⁺ ions in order to achieve the coordination required for catalysis (i.e., coordination of the terminal O3' of the primer strand to the catalytic Mg²⁺ ion). Subsequently, the template DNA strand sequence was modified to 5'-CG*CCATCGCC for the ternary insertion complexes or 5'-GCG*CCATCCCC for the ternary -1 base deletion complexes, with Bz-dG positioned at G*. These sequences parallel that used in a previous MD study on Bz-dG adducted DNA.³² To generate the ternary insertion complexes, Bz-dG was paired opposite each natural dNTP. In each starting complex, four key dihedral angles in the adducted nucleotide (Figure 1) were initially set to the lowest energy orientations previously determined using density functional theory (DFT) calculations on nucleoside models, and MD simulations on adducted DNA helices.³² Specifically, the initial Bz-dG conformation contained $\theta \approx 0^\circ$ (bulky moiety towards N7 of G), $\phi \approx 180^\circ$ (bulky moiety in a planar extended conformation), and $\xi \approx 0^\circ$ (phenyl ring in the same plane as G and the methylene linker). Furthermore, χ was adjusted to the *anti* or *syn* orientation, such that the nascent base pairs considered include *anti*-Bz-dG paired opposite *anti*-dCTP, *anti*-dTTP, *syn*-dGTP, or *syn*-dATP, and *syn*-Bz-dG paired opposite *anti*-dCTP, *anti*-dTTP, *anti*-dATP, or *anti*-dGTP. Additionally, a control simulation was performed for the ternary insertion complex with *anti*-dG at G* paired opposite *anti*-dCTP. To generate the ternary -1 base deletion complexes, no base was positioned opposite *anti* or *syn*-Bz-dG, and dGTP was paired opposite the 5'-dC with respect to the adduct.

The resulting 11 DNA–polymerase complexes were prepared for minimization using the tleap module of Amber 11.⁴⁷ Specifically, hydrogen atoms were added to generate the natural protonation states of all DNA and protein residues. Furthermore, the systems were neutralized with Na⁺ ions and solvated in a TIP3P octahedral water box such that the DNA–polymerase complex was at least 8.0 Å from the edge of the box. The resulting complexes each contain 341 amino acids, a dNTP, 18 (insertion) or 19 (deletion) nucleotides, 2 Mg²⁺ ions, 5 (insertion) or 6 (deletion) Na⁺ ions, and ~900 water molecules. All natural amino acids, nucleotides, and the solvent were modeled with AMBER ff99SB parameters,⁴⁸ while the parameters for Bz-dG³² and the dNTPs⁴⁹⁻⁵¹ were adapted from the literature.

Simulation Procedure: For all systems, the first minimization phase involved 1000 steps of steepest decent minimization, followed by 3000 steps of conjugate gradient minimization, with a 500 kcal mol⁻¹ Å⁻² force constraint on the protein (including the Mg²⁺ ions) and DNA (including the dNTP). Next, the DNA was minimized using 1000 steps of steepest decent minimization, followed by 3000 steps of conjugate gradient minimization, with a 500 kcal mol⁻¹ Å⁻² force constraint on the protein. Finally, 1000 steps of steepest decent minimization, followed by 4000 steps of conjugate gradient minimization, were performed on the entire unconstrained system. Subsequently, the equilibration phase was completed using a Langevin thermostat ($\gamma = 1.0$) to heat the system from 0 to 300 K over 20 ps, with a 10 kcal mol⁻¹ Å⁻² force constraint on the protein and DNA. Finally, a 20 ns unrestrained production MD simulation was performed on each of the 11 systems at 300 K and 1 bar. Each simulation was stable, with an overall backbone root-mean-square deviation (rmsd) of ~1.3–2.3 Å (Table S1). To confirm adequate sampling over the 20 ns, the trajectories for the insertion of *anti*-dCTP opposite *anti*-Bz-dG or *anti*-dG were extended to 100 ns. Extending the simulations led to only small deviations in the structures and do not change the overall conclusions (see Tables S2–S7, and Figures 2–4, S2 and S3 for a comparison of the data), which supports the use of 20 ns trajectories for the remaining systems. Throughout all minimization,

equilibration and production calculations, the periodic boundary condition and a non-bonded cutoff of 10 Å were implemented. Additionally, SHAKE and a 0.002 ps time step were used in all equilibration and production steps. All minimization and equilibration calculations were performed using the sander module of Amber 12, while production simulations were performed using the pmemd module of Amber 12.⁵² Analysis of the MD simulations was completed using AmberTools 14.⁵³ Specifically, the average linear interaction energies for discrete hydrogen-bonding (electrostatic component) and stacking (van der Waals component) interactions of the nascent base pair and 5'/3'-bases with respect to dG* were calculated across the simulation trajectory. Additionally, Molecular Mechanics/Generalized Born Surface Area (MM/GBSA) pairwise energies were calculated for the discrete dNTP–polymerase interactions. We note that it was not feasible to calculate the entropy component of the pairwise energies due to the size of the system. Throughout the paper, average interaction energies are reported with the dynamical information (standard deviations) provided in the Supporting Information. Furthermore, the positions of the nucleobases are referenced with respect to dG*.



R=CH₃, C₂H₂C₆H₅, or C₄H₆OC₅NH₄

Figure S1. Previously reported hydrogen-bonding arrangements between an O6-dG alkylation adduct (namely Me-dG (R=CH₃), Bz-dG (R=C₂H₂C₆H₅), or POB-dG (R=C₄C₆OC₅NH₄)) and (a) dC (wobble base pair) or (b) dT (pseudo Watson-Crick base pair).^{23, 27-32}

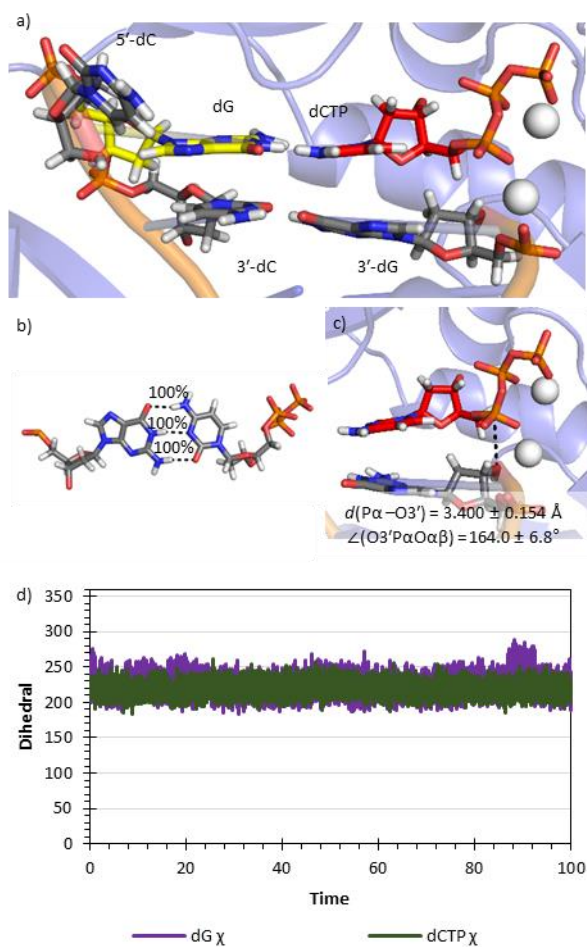


Figure S2. Representative MD structure for the Dpo4 ternary complex of canonical dG replication from 100 ns MD simulations depicting a) the orientation of dCTP with respect to the DNA, b) the dG:dCTP hydrogen-bonding arrangement and the percent occupancy of the hydrogen-bonding interactions, c) the average reaction parameters, and d) the time evolution of key dG and dCTP dihedral angles.

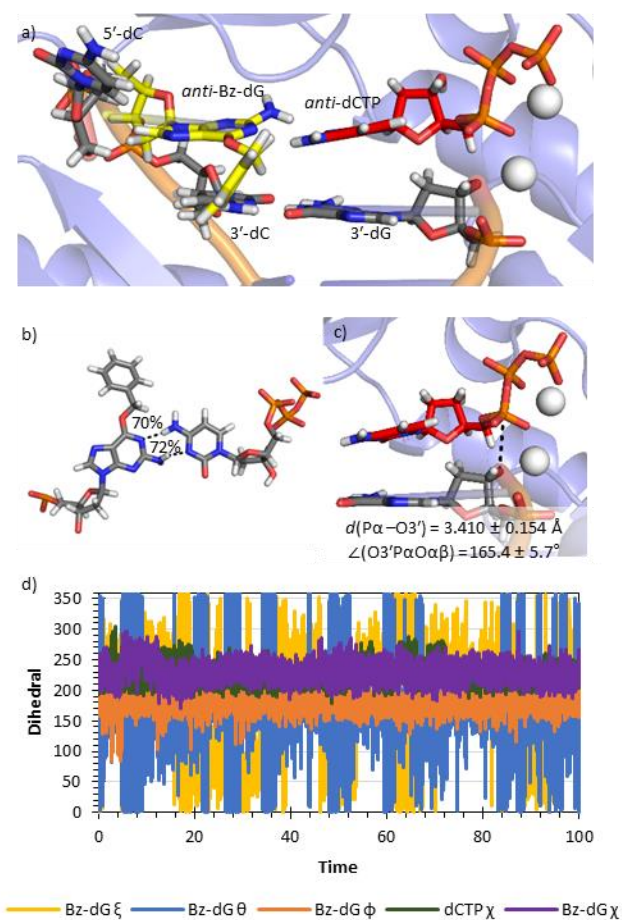


Figure S3. Representative MD structure for the Dpo4 ternary complex of *anti*-Bz-dG replication from 100 ns MD simulations depicting a) the orientation of dCTP with respect to the DNA, b) the *anti*-Bz-dG:dCTP hydrogen-bonding arrangement and the percent occupancy of the hydrogen-bonding interactions, c) the average reaction parameters, and d) the time evolution of key Bz-dG and dCTP dihedral angles.

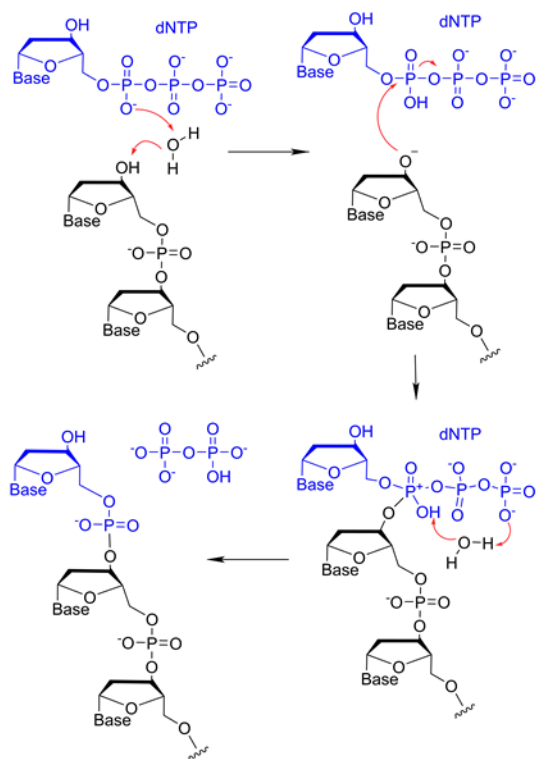


Figure S4. Previously proposed reaction mechanism for the replication of natural DNA by Dpo4.^{54, 55}

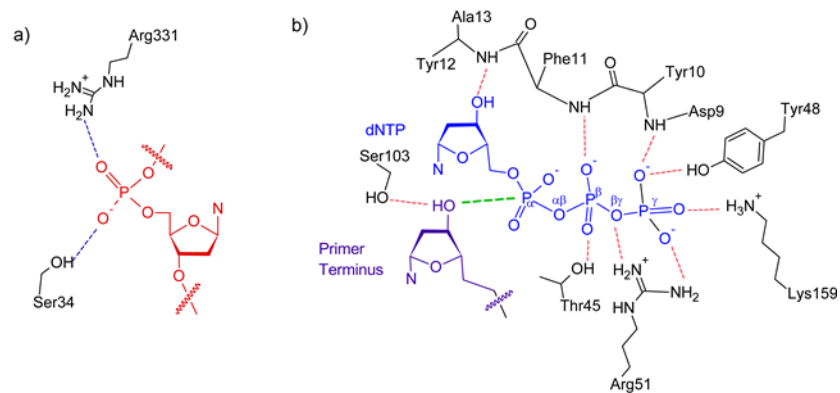


Figure S5. Previously proposed hydrogen-bonding interactions between Dpo4 and a) the base being replicated or b) the dNTP.^{39, 49, 55, 59-61}

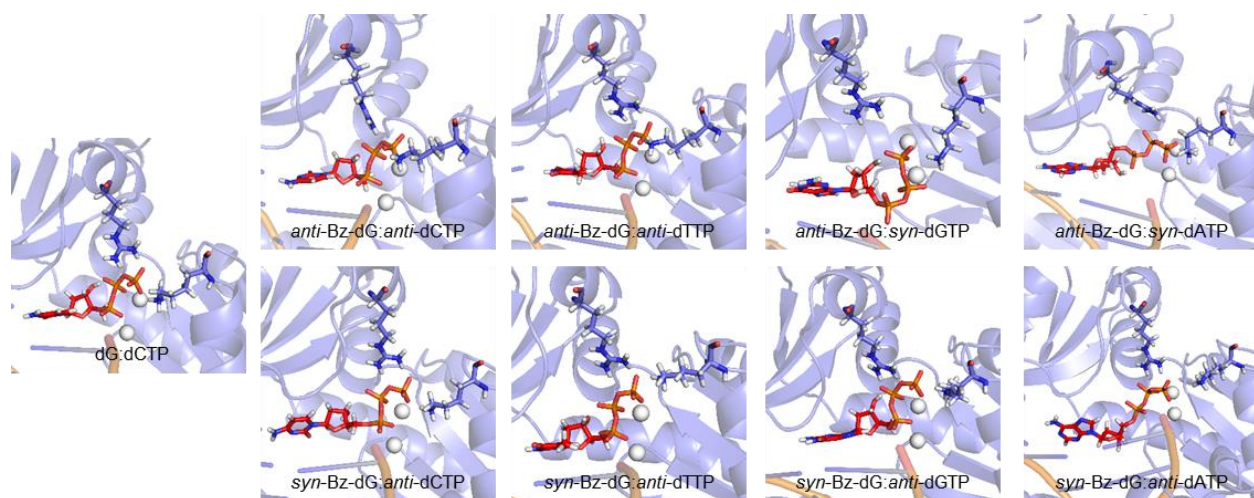


Figure S6. Representative MD structures depicting the orientation of the dNTP with respect to Lys159 and Arg51 in the Dpo4 ternary complex for dG or Bz-dG replication.

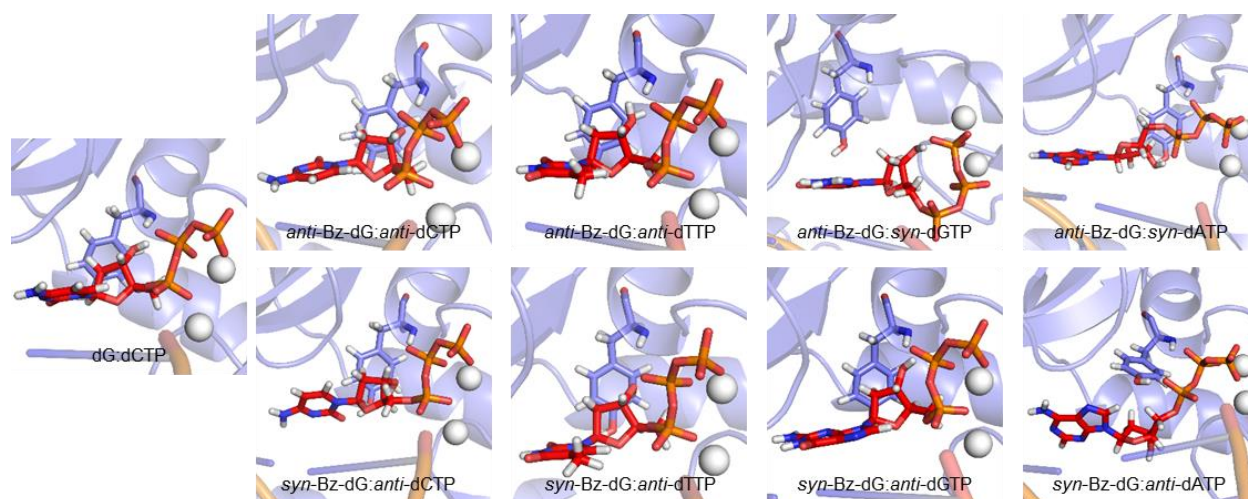


Figure S7. Representative MD structures depicting the orientation of the dNTP with respect to Tyr12 in the Dpo4 ternary complex for dG or Bz-dG replication.

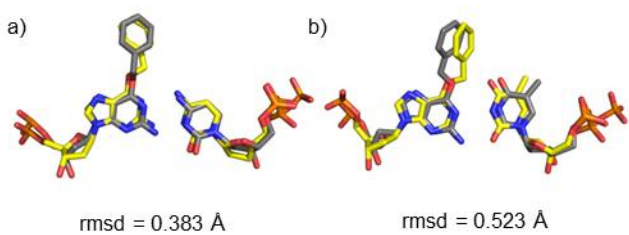


Figure S8. Overlays of MD representative structures from the ternary insertion complexes (grey) and crystal structure of the Dpo4 post-lesion synthesis complex (yellow) for a) Bz-dG:dC (PDB ID: 2JEF) and b) Bz-dG:dT (PDB ID: 2JEI).

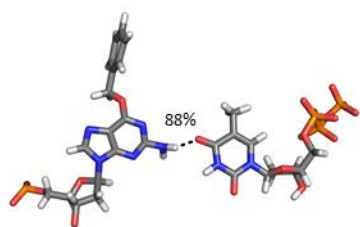


Figure S9. Alternative hydrogen-bonding geometry for the *anti*-Bz-dG:*anti*-dTTP pair formed during the last 11.4 ns of the simulation on the Dpo4 ternary complex.

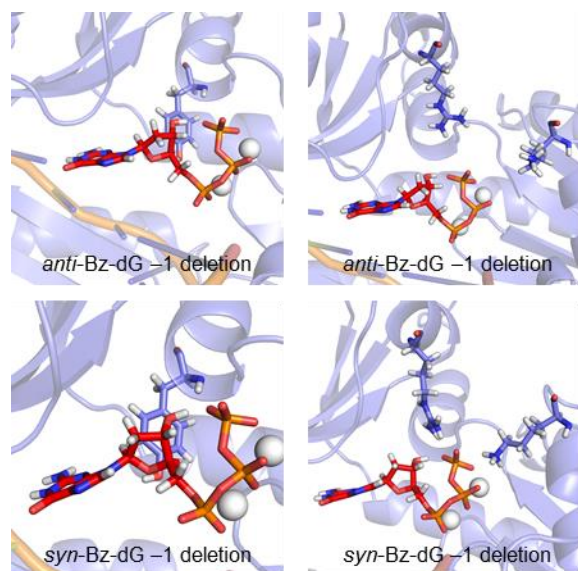


Figure S10. Representative MD structures depicting the orientation of the dNTP with respect to Tyr12 (left) or Arg51 and Lys159 (right) in the Dpo4 ternary -1 deletion complex during *anti* (top) or *syn* (bottom) Bz-dG replication.

Table S1. Backbone rmsds throughout the production MD simulation relative to the first frame for the ternary insertion and deletion complexes for Dpo4 replication of dG or Bz-dG.

Complex	Active Site Base Pair	rmsd
Ternary Insertion	<i>anti</i> -dG: <i>anti</i> -dCTP (20 ns) ^a	1.984±0.296 Å
	<i>anti</i> -dG: <i>anti</i> -dCTP (100 ns) ^a	1.224±0.190 Å
	<i>anti</i> -Bz-dG: <i>anti</i> -dCTP (20 ns) ^a	1.974±0.234 Å
	<i>anti</i> -Bz-dG: <i>anti</i> -dCTP (100 ns) ^a	1.102±0.139 Å
	<i>syn</i> -Bz-dG: <i>anti</i> -dCTP	1.945±0.252 Å
	<i>anti</i> -Bz-dG: <i>anti</i> -dTTP	1.295±0.181 Å
	<i>syn</i> -Bz-dG: <i>anti</i> -dTTP	1.653±0.212 Å
	<i>anti</i> -Bz-dG: <i>syn</i> -dGTP	1.968±0.291 Å
	<i>syn</i> -Bz-dG: <i>anti</i> -dGTP	1.690±0.203 Å
	<i>anti</i> -Bz-dG: <i>syn</i> -dATP	2.338±0.612 Å
	<i>syn</i> -Bz-dG: <i>anti</i> -dATP	2.298±0.435 Å
Deletion	<i>anti</i> -Bz-dG	1.911±0.273 Å
	<i>syn</i> -Bz-dG	1.381±0.254 Å

^a Data from 20 and 100 ns simulations.

Table S2. Structural parameters from MD simulations on the Dpo4 ternary (insertion) replication complexes of dG or Bz-dG.

Active Site Base Pair	dG*	dG*	dG*	dG*	dG*	dNTP	dNTP	dG*:dNTP
	χ^a	Pucker ^b	θ^a	ϕ^a	ξ^a	χ	Pucker ^b	C1'-C1' Distance ^c
<i>anti</i> -dG: <i>anti</i> -dCTP (20 ns) ^d	227.2±14.1°	C1'- <i>exo</i> (40.5%)	NA ^e	NA ^e	NA ^e	216.6±9.5°	C3'- <i>endo</i> (47.8%)	10.824±0.147 Å
<i>anti</i> -dG: <i>anti</i> -dCTP (100 ns) ^d	224.4±15.6°	C1'- <i>exo</i> (39.6%)	NA ^e	NA ^e	NA ^e	219.0±10.2°	C3'- <i>endo</i> (36.5%)	10.809±0.142 Å
<i>anti</i> -Bz-dG: <i>anti</i> -dCTP (20 ns) ^d	230.1±16.9°	C1'- <i>exo</i> (43.4%)	168.9±69.4°	178.4±13.7°	185.1±93.6°	226.1±15.9°	C1'- <i>exo</i> (30.9%)	11.669±0.419 Å
<i>anti</i> -Bz-dG: <i>anti</i> -dCTP (100 ns) ^d	233.1±19.7°	C1'- <i>exo</i> (26.0%)	163.9±83.5°	179.0±13.7°	260.5±56.4°	224.2±14.9°	C1'- <i>exo</i> (27.0%)	11.490±0.404 Å
<i>syn</i> -Bz-dG: <i>anti</i> -dCTP	48.2±13.3°	C1'- <i>exo</i> (75.8%)	209.3±84.0°	177.1±9.9°	145.6±90.7°	246.9±17.6°	C1'- <i>exo</i> (50.0%)	11.094±0.302 Å
<i>anti</i> -BzG: <i>anti</i> -TTP (pseudo Watson-Crick) ^f	248.7±13.4°	C3'- <i>exo</i> (62.2%)	87.2±90.5°	193.6±15.1°	23.3±94.6°	219.3±10.9°	C3'- <i>endo</i> (48.2%)	10.815±0.229 Å
<i>anti</i> -BzG: <i>anti</i> -TTP (alternative hydrogen bonding) ^f	254.4±11.1°	C3'- <i>exo</i> (34.5%)	84.4±120.7°	182.6±13.9°	351.2±90.8°	216.4±10.7°	C3'- <i>endo</i> (48.3%)	11.571±0.335 Å
<i>syn</i> -Bz-dG: <i>anti</i> -dTTP	47.1±11.2°	C1'- <i>exo</i> (35.4%)	154.4±120.0°	179.1±17.3°	189.8±102.8°	216.7±10.0°	C3'- <i>endo</i> (39.4%)	11.950±0.388 Å
<i>anti</i> -Bz-dG: <i>syn</i> -dGTP	244.8±25.3°	C2'- <i>exo</i> (36.2%)	167.2±93.4°	194.9±41.9°	189.1±94.3°	12.8±21.5°	C1'- <i>exo</i> (40.7%)	11.541±2.044 Å
<i>syn</i> -Bz-dG: <i>anti</i> -dGTP	40.0±13.2°	C3'- <i>endo</i> (58.3%)	186.9±58.2°	164.2±47.4°	165.1±98.8°	240.9±10.9°	C3'- <i>endo</i> (70.4%)	12.460±0.403 Å
<i>anti</i> -Bz-dG: <i>syn</i> -dATP	256.8±12.7°	C2'- <i>exo</i> (56.3%)	145.0±52.2°	183.9±40.6°	174.1±94.9°	321.7±15.5°	C1'- <i>exo</i> (72.2%)	9.597±0.318 Å
<i>syn</i> -Bz-dG: <i>anti</i> -dATP	53.1±11.8°	C1'- <i>exo</i> (33.1%)	168.7±73.2°	164.0±65.6°	152.0±96.2°	212.3±25.0°	C2'- <i>endo</i> (45.3%)	10.004±0.856 Å

^a dG* dihedral angle (degrees). See Figure 1 for definitions of adduct dihedral angles. ^b Most common sugar pucker of dG* or the dNTP, and the percentage of the simulation that the sugar pucker is adopted. ^c Width of the dG* base pair. ^d Data from 20 and 100 ns simulations. ^e Not applicable. ^f See Figures 4 and S9 for a description of the different *anti*-BzG:*anti*-TTP hydrogen-bonding orientations.

Table S3. Occupancies of the hydrogen bonds in the 3' and 5' flanking base pairs in MD simulations on the ternary insertion and deletion complexes for Dpo4 replication of dG or Bz-dG.

Complex	Active Site Base Pair	Location ^a	O6...HN4 ^b	N1H...N3 ^b	N2H...O2 ^b
Ternary Insertion	<i>anti</i> -dG: <i>anti</i> -dCTP (20 ns) ^c	3'	100%	100%	100%
	<i>anti</i> -dG: <i>anti</i> -dCTP (100 ns) ^c	3'	100%	100%	100%
	<i>anti</i> -Bz-dG: <i>anti</i> -dCTP (20 ns) ^c	3'	92%	98%	100%
	<i>anti</i> -Bz-dG: <i>anti</i> -dCTP (100 ns) ^c	3'	99%	99%	100%
	<i>syn</i> -Bz-dG: <i>anti</i> -dCTP	3'	98%	100%	100%
	<i>anti</i> -BzG: <i>anti</i> -TTP (pseudo Watson-Crick) ^d	3'	98%	100%	100%
	<i>anti</i> -BzG: <i>anti</i> -TTP (alternative hydrogen bonding) ^d	3'	90%	98%	100%
	<i>syn</i> -Bz-dG: <i>anti</i> -dTTP	3'	70%	77%	99%
	<i>anti</i> -Bz-dG: <i>syn</i> -dGTP	3'	90%	97%	100%
	<i>syn</i> -Bz-dG: <i>anti</i> -dGTP	3'	98%	100%	100%
	<i>anti</i> -Bz-dG: <i>syn</i> -dATP	3'	98%	100%	100%
	<i>syn</i> -Bz-dG: <i>anti</i> -dATP	3'	60%	59%	58%
	Deletion	<i>anti</i> -Bz-dG	3'	99%	99%
		5'	100%	100%	99%
<i>syn</i> -Bz-dG		3'	96%	100%	99%
		5'	100%	99%	99%

^a Location with respect to dG*. ^b Hydrogen-bonding occupancies are based on a distance cutoff of < 3.4 Å and an angle cutoff of < 120°. ^c Data from 20 and 100 ns simulations. ^d See Figures 4 and S9 for a description of the different *anti*-BzG:*anti*-TTP hydrogen-bonding orientations.

Table S4. Linear interaction energies (kJ mol⁻¹) for stacking and hydrogen-bonding interactions between dG* and the flanking base pairs in MD simulations on the ternary complexes for Dpo4 replication of dG or Bz-dG.

Active Site Base Pair	3' Hydrogen Bonding ^a	dG*:dNTP Interaction ^b	3' Stacking ^c	5' Stacking ^c
<i>anti</i> -dG: <i>anti</i> -dCTP (20 ns) ^d	-122.0±10.6	-127.6±11.3	-62.9±4.0	-1.0±1.2
<i>anti</i> -dG: <i>anti</i> -dCTP (100 ns) ^d	-114.9±31.7	-125.1±24.3	-61.8±8.2	-1.0±0.9
<i>anti</i> -Bz-dG: <i>anti</i> -dCTP (20 ns) ^d	-116.2±14.2	-23.0±11.7	-62.7±5.8	-1.3±2.4
<i>anti</i> -Bz-dG: <i>anti</i> -dCTP (100 ns) ^d	-119.3±12.7	-23.9±12.2	-61.9±6.1	-6.9±7.4
<i>syn</i> -BzG: <i>anti</i> -CTP	-117.2±17.2	-29.3±10.9	-60.5±5.8	-6.2±2.7
<i>anti</i> -BzG: <i>anti</i> -TTP (pseudo Watson-Crick) ^e	-120.6±7.4	-16.1±7.9	-69.7±4.6	-3.7±4.5
<i>anti</i> -BzG: <i>anti</i> -TTP (alternative hydrogen bonding) ^e	-113.9±13.8	-8.3±6.7	-64.4±4.9	-17.1±5.2
<i>syn</i> -BzG: <i>anti</i> -TTP	-102.7±24.6	0.8±2.9	-50.3±7.2	-25.2±5.3
<i>syn</i> -BzG: <i>anti</i> -GTP	-117.1±11.5	2.1±1.7	-47.3±4.6	-26.3±4.5
<i>anti</i> -BzG: <i>syn</i> -GTP	-115.3±14.9	-24.7±18.4	-61.6±7.8	-11.4±8.3
<i>anti</i> -BzG: <i>syn</i> -ATP	-120.7±11.4	-13.4±7.5	-45.7±5.2	-15.5±5.7
<i>syn</i> -BzG: <i>anti</i> -ATP	-76.3±48.5	-6.3±4.2	-40.6±7.5	-5.7±5.5

^aStrength of the hydrogen bond in the base pair 3' with respect to dG*. ^bStrength of the interaction between dG* and the pairing dNTP. ^cStrength of the stacking interaction between the dG base pair and the base pair 5' or 3' with respect to dG*. ^dData from 20 and 100 ns simulations. ^eSee Figures 4 and S9 for a description of the different *anti*-BzG:*anti*-TTP hydrogen-bonding orientations.

Table S5. Occupancies of the hydrogen bonds between Dpo4 and the incoming dNTP or G* in MD simulations on the Dpo4 ternary complexes for dG or Bz-dG replication. ^{a,b}

Acceptor	Donor	<i>anti</i> -dG: <i>anti</i> -dCTP			<i>anti</i> -Bz-dG: <i>anti</i> -dCTP			<i>syn</i> -Bz-dG: <i>anti</i> -dCTP			<i>anti</i> -Bz-dG: <i>anti</i> -dTTP			<i>syn</i> -Bz-dG: <i>anti</i> -dTTP			<i>anti</i> -Bz-dG: <i>syn</i> -dGTP			<i>syn</i> -Bz-dG: <i>anti</i> -dGTP			<i>anti</i> -Bz-dG: <i>syn</i> -dATP			<i>syn</i> -Bz-dG: <i>anti</i> -dATP		
		%	Å	Deg.	%	Å	Deg.	%	Å	Deg.	%	Å	Deg.	%	Å	Deg.	%	Å	Deg.	%	Å	Deg.	%	Å	Deg.	%	Å	Deg.
dG*(O3')	Ser34(OyH)	8%	2.8	152.6	NO ^b			12%	3.2	131.4	NO ^b			NO ^b			NO ^b			6%	2.9	149.9	54%	3.1	145.3			
dG*(OP2)	Arg331(NeH)	14%	3.3	135.5	9%	3.2	135.9	6%	3.0	151.8	35%	3.0	156.3	24%	3.2	139.3	28%	3.0	156.0	15%	3.2	138.1	88%	2.9	153.6	12%	3.2	140.9
dG*(OP1)	Arg331(NηH)	98%	2.8	161.8	92%	2.8	161.1	61%	3.0	154.2	46%	2.9	153.6	100%	2.8	163.0	50%	3.0	152.0	100%	2.8	164.2	NO ^b			76%	2.9	157.2
dG*(OP2)	Arg331(NηH)	NO ^b			NO ^b			NO ^b			65%	2.8	157.5	NO ^b			29%	2.9	158.1	NO ^b			88%	2.8	162.3	NO ^b		
dG*(OP)	Gly41(NH)	12%	3.0	138.0	34%	3.0	142.5	59%	3.0	143.5	NO ^b			NO ^b			42%	3.0	139.6	NO ^b			NO			63%	3.0	142.3
dG*(OP1)	Ser34(OyH)	36%	2.8	162.4	64%	2.8	160.8	NO ^b			30%	2.7	164.1	100%	2.7	164.9	NO ^b			100%	2.7	164.9	8%	2.7	162.9	34%	2.9	157.0
dG*(OP2)	Ser34(OyH)	NO ^b			22%	2.9	162.5	76%	2.8	164.6	NO ^b			NO ^b			60%	2.8	164.3	NO ^b			NO ^b			45%	2.9	159.3
dGTP(N7)	Tyr12(OH)	NO ^b			NO ^b			NO ^b			NO ^b			NO ^b			36%	3.0	152.5	NO ^b			NO ^b			NO ^b		
dNTP(O3')	Tyr12(OH)	NO ^b			NO ^b			NO ^b			NO ^b			83%	3.1	162.8	34%	2.8	161.5	NO ^b			5%	3.1	136.2	NO ^b		
dNTP(O3')	Tyr12(NH)	79%	3.1	162.9	86%	3.1	162.3	23%	3.2	160.5	81%	3.1	163.6	NO ^b			NO ^b			87%	3.1	165.5	NO ^b			NO ^b		
dNTP(O5')	Tyr12(OH)	NO ^b			NO ^b			NO ^b			NO ^b			NO ^b			NO ^b			NO ^b			NO ^b			18%	3.2	144.2
dNTP(O5')	dG 3'(O3')	NO ^b			NO ^b			NO ^b			NO ^b			NO ^b			NO ^b			98%	2.7	161.7	NO ^b			NO ^b		
dNTP(Oα1)	Tyr12(OH)	NO ^b			NO ^b			NO ^b			NO ^b			NO ^b			NO ^b			NO ^b			NO ^b			36%	3.0	158.5
dNTP(Oβ3)	Arg51(NηH)	74%	2.9	159.6	97%	2.9	161.0	82%	2.9	159.1	100%	2.9	161.3	100%	2.9	161.5	NO ^b			90%	3.0	141.4	NO ^b			NO ^b		
dNTP(Oβ)	Lys152(NζH)	NO ^b			NO ^b			94%	2.8	156.6	NO ^b			NO ^b			21%	2.9	139.1	NO ^b			NO ^b			NO ^b		
dNTP(Oβ)	Lys159(NζH)	NO ^b			NO ^b			NO ^b			NO ^b			NO ^b			34%	3.0	132.4	NO ^b			NO ^b			NO ^b		
dNTP(Oβ2)	Phe11(NH)	67%	3.2	158.9	54%	3.3	158.3	44%	3.2	157.9	58%	3.3	158	59%	3.3	156.8	NO ^b			99%	3.1	160.9	67%	3.1	156.6	70%	3.1	156.3
dNTP(Oβ1)	Thr45(OyH)	100%	2.7	162.4	100%	2.7	163.0	100%	2.7	163.5	100%	2.7	163.0	100%	2.7	163.8	NO ^b			10%	3.0	146.7	NO ^b			77%	2.7	165.8
dNTP(Oβ3)	Tyr10(NH)	NO ^b			NO ^b			35%	3.0	126.5	42%	3.1	125.9	46%	3.0	126.1	NO ^b			56%	2.9	129.4	13%	3.2	135.7	NO ^b		
dNTP(Oy3)	Arg51(NηH2)	57%	3.0	143.6	51%	3.1	137.0	55%	3.0	143.3	44%	3.2	135.9	NO ^b			30%	3.2	138.6									
dNTP(Oy2)	Arg51(NηH2)	NO ^b			NO ^b			6%	3.3	134.2	NO ^b			23%	3.2	136.1	52%	2.8	156.4	13%	3.2	138.1	NO ^b			41%	3.2	157.4
dNTP(Oy3)	Arg51(NηH1)	84%	2.9	154.7	88%	2.8	159.9	88%	2.9	152.9	81%	2.8	161.1	64%	3.0	150.0	NO ^b			NO ^b			NO ^b			65%	2.9	164.2
dNTP(Oy2)	Arg51(NηH1)	51%	3.0	150.3	35%	3.0	148.3	62%	3.1	148.1	38%	3.0	153.3	69%	3.0	158.2	45%	2.9	148.0	97%	2.8	164.2	NO ^b			NO ^b		
dNTP(Oy1)	Lys159(NζH)	37%	2.9	154.3	19%	2.9	152.6	NO ^b			NO ^b			77%	2.8	152.3	51%	2.8	156.0	58%	2.8	136.5	77%	2.8	158.1	NO ^b		
dNTP(Oy2)	Lys159(NζH)	NO ^b			NO ^b			NO ^b			NO ^b			NO ^b			NO ^b			87%	2.9	157.7	NO ^b			NO ^b		
dNTP(Oy3)	Lys159(NζH)	69%	2.8	154.1	75%	2.8	157.5	29%	3.1	138.7	93%	2.8	157.8	41%	3.0	149.6	47%	2.8	161.6	NO ^b			NO ^b			NO ^b		
dNTP(Oy3)	Tyr10(NH)	100%	2.9	162.4	99%	2.9	167.1	100%	2.9	164.3	99%	2.9	167.6	100%	2.9	167.3	11%	3.1	139.1	49%	3.2	163	NO ^b			62%	3.0	136.4
dNTP(Oy3)	Tyr48(OH)	24%	2.7	164.4	NO			40%	2.8	159.6	NO			84%	2.6	165.5	26%	2.7	165.8	98%	2.7	167.6	25%	2.7	163.0	NO ^b		
Gly58(O)	Bz-dG(N2H)	NO ^b			NO ^b			NO ^b			NO ^b			NO ^b			34%	3.0	141.7	NO ^b			24%	3.0	143.5	NO ^b		

^a Hydrogen-bonding occupancies are based on a distance cutoff of < 3.4 Å and an angle cutoff of > 120°. ^b Not observed.

Table S6. MM/GBSA average pairwise energy contributions of individual residues to dNTP binding (kJ mol^{-1}) during MD simulations on the Dpo4 ternary complexes for dG or Bz-dG replication. ^a

Active Site Base Pair	Mg343	Mg342	Arg51	Lys159	Tyr10	Thr45	Phe11	Ala44	Gln14	Tyr12	Tyr48	Ile104	Lys152	Asp9	Lys78
<i>anti</i> -dG: <i>anti</i> -dCTP (20 ns) ^b	-937.1	-435.7	-191.4	-127.7	-58.2	-45.5	-28.8	-18.4	-15.6	-15.3	-14.7	-10.7	-10.0	-8.6	-1.9
<i>anti</i> -dG: <i>anti</i> -dCTP (100 ns) ^b	-930.4	-429.7	-178.3	-148.3	-57.7	-45.1	-27.0	-18.2	-15.8	-14.6	-6.3	-10.1	-10.3	-6.6	-1.8
<i>anti</i> -Bz-dG: <i>anti</i> -dCTP (20 ns) ^b	-918.7	-430.2	-185.7	-116.0	-57.8	-45.2	-27.1	-17.1	-15.0	-16.7	-15.5	-10.8	-12.1	-10.1	-6.2
<i>anti</i> -Bz-dG: <i>anti</i> -dCTP (100 ns) ^b	-907.4	-419.7	-187.3	-121.5	-58.5	-46.2	-27.4	-18.2	-15.0	-18.0	-17.4	-10.3	-13.1	-10.7	-3.3
<i>syn</i> -Bz-dG: <i>anti</i> -dCTP	-1056.7	-451.9	-193.6	-174.9	-57.9	-45.0	-24.5	-16.1	-16.0	-21.7	-20.8	-13.5	-9.1	-4.9	-18.3
<i>anti</i> -Bz-dG: <i>anti</i> -dTTP	-884.8	-390.0	-181.9	-114.8	-58.0	-44.6	-26.8	-18.5	-14.6	-16.1	-16.4	-9.5	-6.0	-11.3	-1.4
<i>syn</i> -Bz-dG: <i>anti</i> -dTTP	-991.4	-412.6	-188.0	-203.0	-59.8	-46.0	-27.9	-18.8	-18.8	-17.0	-43.3	-9.4	-8.9	13.4	-2.2
<i>anti</i> -Bz-dG: <i>syn</i> -dGTP	-661.9	-732.8	-58.9	-135.2	-13.7	-5.8	-6.5	-12.2	-3.8	-14.1	-0.9	-5.3	-30.8	-1.1	-6.6
<i>syn</i> -Bz-dG: <i>anti</i> -dGTP	-1154.7	-397.3	-119.1	-216.4	-48.5	-16.5	-43.3	-17.7	-14.9	-19.7	-46.7	-10.1	-6.4	13.9	-0.9
<i>anti</i> -Bz-dG: <i>syn</i> -dATP	-910.7	-437.6	-17.7	-80.1	-27.8	-10.4	-21.0	-15.4	-8.8	-8.8	-0.6	-4.0	-2.4	-0.5	-1.7
<i>syn</i> -Bz-dG: <i>anti</i> -dATP	-999.1	-546.4	-110.2	-13.1	-39.0	-40.7	-23.7	-13.9	-9.3	-30.1	1.1	-14.7	-8.3	-0.8	-11.5
<i>anti</i> -Bz-dG deletion	-896.2	-422.8	-18.9	-19.4	-9.9	-6.6	-4.8	-7.3	-1.9	0.2	0.1	-4.2	-6.8	-0.8	-2.5
<i>syn</i> -Bz-dG deletion	-970.6	-614.5	-26.9	-81.2	-11.6	-9.0	-3.6	-15.0	-2.1	-7.2	0.1	-7.8	-19.0	-7.9	-1.7

^a Only residues that contributed more than 10 kJ mol^{-1} to dNTP binding are reported. ^b Data from 20 and 100 ns simulations.

Table S7. Coordination of catalytic Mg²⁺ ions during MD simulations on the ternary complex for dG or Bz-dG replication. ^a

Active Site Base Pair	Catalytic Ion: Mg342					Nucleotide Binding Ion: Mg343						
	Primer(O3')	Glu106(Oε1)	Asp7(Oδ1)	dNTP(Oα2)	Asp105(Oδ1)	Wat(O)	Asp7(Oδ2)	Phe8(O)	Asp105(Oδ2)	dNTP(Oα2)	dNTP(Oβ2)	dNTP(Oγ1)
<i>anti</i> -dG: <i>anti</i> -dCTP (20 ns) ^b	94%	100%	100%	99%	100%	100%	100%	100%	100%	8%	100%	100%
<i>anti</i> -dG: <i>anti</i> -dCTP (100 ns) ^b	98%	100%	100%	100%	100%	100%	100%	100%	100%	5%	100%	100%
<i>anti</i> -Bz-dG: <i>anti</i> -dCTP (20 ns) ^b	97%	100%	100%	100%	100%	100%	100%	100%	100%	10%	100%	100%
<i>anti</i> -Bz-dG: <i>anti</i> -dCTP (100 ns) ^b	98%	100%	100%	100%	100%	100%	100%	100%	100%	4%	100%	100%
<i>syn</i> -Bz-dG: <i>anti</i> -dCTP	93%	100%	100%	92%	100%	100%	100%	100%	100%	62%	100%	100%
<i>anti</i> -BzG: <i>anti</i> -TTP (pseudo Watson-Crick) ^d	98%	100%	100%	99%	100%	100%	100%	100%	100%	15%	100%	100%
<i>anti</i> -BzG: <i>anti</i> -TTP (alternative hydrogen bonding) ^d	98%	100%	100%	100%	100%	100%	100%	100%	100%	0%	100%	100%
<i>syn</i> -Bz-dG: <i>anti</i> -dTTP	100%	100%	100%	97%	100%	100%	100%	100%	100%	33%	100%	100%
<i>anti</i> -Bz-dG: <i>syn</i> -dGTP	NO ^c	NO ^c	100%	NO ^c	100%	42%	100%	100%	100%	NO ^c	NO ^c	100%
<i>syn</i> -Bz-dG: <i>anti</i> -dGTP	99%	100%	100%	97%	100%	100%	100%	100%	100%	97%	100%	100%
<i>anti</i> -Bz-dG: <i>syn</i> -dATP	1%	100%	100%	NO ^c	100%	100%	100%	100%	100%	NO ^c	100%	NO ^c
<i>syn</i> -Bz-dG: <i>anti</i> -dATP	100%	100%	100%	NO ^c	100%	100%	NO ^c	100%	100%	NO ^c	100%	100%
<i>anti</i> -Bz-dG Deletion	NO ^c	NO ^c	76%	NO ^c	NO ^c	NO ^c	NO ^c	NO ^c	NO ^c	100%	100%	NO ^c
<i>syn</i> -Bz-dG Deletion	NO ^c	NO ^c	100%	NO ^c	NO ^c	NO ^c	NO ^c	NO ^c	NO ^c	100%	100%	NO ^c

^a Percentage of the simulation that the distance between the Mg²⁺ ion and the specified atom is < 2.5 Å. ^b Data from 20 and 100 ns simulations. ^c Not observed. ^d See Figures 4 and S9 for a description of the different *anti*-BzG:*anti*-TTP hydrogen-bonding orientations.

Table S8. Structural parameters from MD simulations on the Dpo4 –1 base deletion complex for Bz-dG replication.

G*	rmsd	G* Pucker ^a	G* χ^b	G* θ^b	G* ϕ^b	G* ξ^b	5' Base Pair C1'–C1' Distance ^c	3' Base Pair C1'–C1' Distance ^c	Reaction Distance ^d	Reaction Angle ^e
<i>anti</i> -Bz-dG	1.911±0.273 Å	C4'- <i>exo</i> (53.2%)	226.2±8.8°	178.5±132.2°	159.5±43.7°	176.9±88.6°	10.951±0.222 Å	10.831±0.178 Å	5.630±0.492 Å	84.3±15.8°
<i>syn</i> -Bz-dG	1.381±0.254 Å	O4'- <i>endo</i> (50.9%)	58.1±19.2°	182.3±94.3°	223.7±49.1°	204.1±95.6°	10.874±0.195 Å	10.685±0.195 Å	4.801±1.019 Å	103.1±16.2°

^a Most common sugar pucker of Bz-dG and the percentage of the simulation that the sugar pucker is adopted. ^b Bz-dG dihedral angle (degrees). See Figure 1 for definitions of adduct dihedral angles. ^c Width of the base pair 5' or 3' with respect to Bz-dG. ^d Distance between O3'(primer 3' end) and P α (dNTP). ^e $\angle(O3'(primer\ 3'\ end)-P\alpha(dNTP)-O\alpha\beta(dNTP))$.

Table S9. Strength (kJ mol^{-1}) of stacking and hydrogen-bonding interactions involving Bz-dG and the flanking base pairs in MD simulations on the Dpo4 -1 base deletion complex for Bz-dG replication.

G*	3' Base Pair Hydrogen Bond ^a	5' Base Pair Hydrogen Bond ^a	5' Stacking ^b	3' Stacking ^b
<i>anti</i> -Bz-dG	-110.0±8.3	-116.5±8.2	-15.4±8.2	-41.0±13.9
<i>syn</i> -Bz-dG	-111.2±6.9	-113.4±11.1	-14.5±9.2	-39.8±14.3

^a Strength of the hydrogen bond in the base pair 5' or 3' with respect to Bz-dG. ^b Strength of the stacking interaction between Bz-dG and the 5' or 3' inter and intrastand bases with respect to Bz-dG

Table S10. Occupancies for the hydrogen bonds between Dpo4 and the incoming dNTP or the dC being replicated in MD simulations on the Dpo4 deletion complexes for Bz-dG replication. ^a

Acceptor	Donor	<i>anti</i> -Bz-dG			<i>syn</i> -Bz-dG		
		%	Å	Deg.	%	Å	Deg.
dC354(OP)	Ser34(O γ H)	79%	2.9	159.3	55%	2.9	162.8
dC354(OP)	Ser40(O γ H)	NO ^b			7%	2.7	158.2
dC354(OP)	Arg331(N η H)	70%	3.0	153.4	86%	2.9	160.7
dC354(OP)	Arg36(N η H)	27%	2.9	156.5	NO ^b		
Ala44(O)	dGTP(O3')	NO ^b			9%	2.9	156.7
dGTP(O3')	Thr45(O γ H)	11%	2.8	160.5	8%	3.0	161.3
dGTP(O γ)	Tyr10(NH)	10%	3.0	145.2	NO ^b		
dGTP(O γ)	Arg51(N η H)	16%	2.9	151.2	16%	2.8	164.0
dGTP(O γ)	Lys159(N ζ H)	NO ^b			74%	2.8	157.0
dGTP(O γ)	Tyr10(NH)	NO ^b			16%	3.0	157.9

^a Hydrogen-bonding occupancies are based on a distance cutoff of < 3.4 Å and an angle cutoff of > 120°. ^b Not observed.